THE JOURNAL OF PHYSICAL CHEMISTRY Letters

pubs.acs.org/JPCL

Letter

Interfacial Concentration Effect Facilitates Heterogeneous Nucleation from Solution

David McKechnie, Samira Anker, Saraf Zahid, Paul A. Mulheran, Jan Sefcik, and Karen Johnston*

Cite This: *J. Phys. Chem. Lett.* 2020, 11, 2263−2271

Read Online

ACCESS | Metrics & More | Article Recommendations | Supporting Information

ABSTRACT: Crystal nucleation from solution plays an important role in environmental, biological, and industrial processes and mainly occurs at interfaces, although the mechanisms are not well understood. We performed nucleation experiments on glycine aqueous solutions and found that an oil−solution interface dramatically accelerates glycine nucleation compared to an air−solution interface. This is surprising given that nonpolar, hydrophobic oil (tridecane) would not be expected to favor heterogeneous nucleation of highly polar, hydrophilic glycine. Molecular dynamics simulations found significantly enhanced vs depleted glycine concentrations at the oil−solution vs air−solution interfaces, respectively. We propose that this interfacial concentration effect facilitates heterogeneous nucleation, and that it is due to dispersion interactions. This interface effect is distinct from previously described mechanisms, including surface functionalization, templating, and confinement and is expected to be present in a wide range of solution systems. This work provides new insight that is essential for understanding and controlling heterogeneous nucleation.

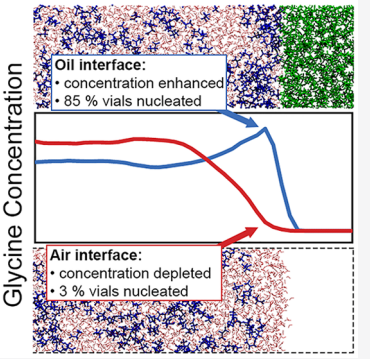

Nucleation is a ubiquitous phenomenon that plays an important role in many environmental, biological, and industrial processes such as ice formation in the atmosphere,[1,2] crystallization of cataracts and kidney stones,[3−5] and development of new pharmaceutical and chemical products.[6] However, nucleation still presents a major scientific challenge as we have only a limited understanding of how crystals are formed, and therefore we cannot accurately control or meaningfully predict what crystal form will nucleate, how fast, in what location, and under what conditions.[7] Understanding of nucleation would enable better control over crystallization processes. It is widely accepted that crystal nucleation from solutions often occurs via heterogeneous mechanisms. A number of possible mechanisms have been considered to explain why heterogeneous nucleation is often faster than homogeneous nucleation.[8] According to classical nucleation theory, heterogeneous nucleation is faster due to a lower crystal surface energy resulting in a reduced energy barrier to nucleation. Specific interfacial effects that favor heterogeneous nucleation include chemical functionality of the interface in contact with solution, physical templating, and confinement. Chemical functionality of the interface leads to specific interactions between these functional groups and the solute molecules, resulting in binding and/or orientation of the solute at the interface.[9] Physical templating, or epitaxy, induces spatial ordering of the solute molecule at the interface.[10] There have been numerous studies investigating the effect of confinement on nucleation in a wide range of systems and it was found that confinement can increase or decrease nucleation rates through a number of underlying mechanisms.[1,11] For heterogeneous nucleation it is generally assumed that the concentration near the interface is the same as in the bulk. However, in this work we challenge this assumption and show that the interfacial concentration can significantly depend on the nature of the interface, even in the absence of any specific interactions, thus facilitating heterogeneous nucleation.

Interfacial effects on nucleation become increasingly prominent with decreasing solution volume, as surface-to-volume ratio increases inversely with the container size. High throughput experiments with a large number of small samples, such as microfluidics and microplates, are becoming increasingly common in nucleation studies to obtain large amounts of data using less material and time. A number of different microfluidic devices[12−15] have been developed for the purpose of investigating crystallization behavior. These devices have been used to investigate the nucleation of water,[16] proteins,[13,17] and small organic molecules.[14,18] Another small scale experimental setup uses a microplate to store a large number of small volumes of solutions[19,20] to observe their crystallization behavior. As these are open to the air, the solution is typically covered by oil to prevent evaporation, similarly to microfluidics, where immiscible liquid is used to separate microdroplets.

Received: February 18, 2020
Accepted: February 28, 2020
Published: February 28, 2020

https://dx.doi.org/10.1021/acs.jpclett.0c00540
J. Phys. Chem. Lett. 2020, 11, 2263−2271

This raises questions about the role of vessel surfaces, which become paramount in small scale experiments, and transferability of these data to larger scales where interfaces may be different and less important. Ildefonso et al. demonstrated that discrepancies in nucleation rates of lysosyme reported in the literature can be related to the interfacial energies of the oils used within the microfluidic setups.[21] It has been observed that the nucleation rate of isonicotinamide in ethanol is orders of magnitude larger when measured in a microfluidic setup with fluorinated oil in comparison to glass vials.[22] Recent work showed that the presence of a PTFE stirrer bar greatly increased the nucleation rate of glycine from aqueous solution in quiescent, isothermal conditions.[23] It is therefore crucial to understand what is the effect of supposedly inert interfaces, such as oils used in microfludics and microplate setups and polymer wells, tubings or stirrers in nucleation experiments, and what are underlying nucleation mechanisms.

In this work we demonstrate the impact of an oil−solution interface on nucleation behavior using aqueous glycine solution in contact with a layer of tridecane. We have performed a large number of small scale experiments at several glycine concentrations with and without a tridecane layer present. We observed a significant increase in the nucleation rate of glycine when the liquid−liquid interface is present even at low supersaturation. Specific interactions between the interface and the functional groups of the solute are unlikely due to the interface being between a simple alkane and aqueous glycine solution, and neither epitaxy nor confinement apply due to the flat liquid nature of the interface. That raises a question of what is the reason for this effect. To further investigate the effects of the liquid−liquid interface, we employed classical molecular dynamics (MD) simulations. While time and length scale limitations mean that rare events such as nucleation are typically inaccessible in standard MD simulations, they can be used to investigate details of glycine solutions at the tridecane interface, including local concentration and ordering of glycine molecules in order to explain the vastly increased nucleation rate at the interface.

We used glycine powder (Sigma-Aldrich, for electrophoresis ≥99%), tridecane (Sigma-Aldrich, ≥99%), and deionized water from an in-house dispenser (Milli-Q, 18.2 MΩ cm).

Samples were prepared using two different methods in order to determine the impact of the preparation method on nucleation behavior. Method one involved glycine solution being prepared directly within individual vials in order to avoid issues related to transferring solutions at high temperatures, such as those discussed by Little et al.,[20] which resulted in data with low reproducibility. Vials were prepared at a range of concentrations from 275 to 450 $g_{glycine}/kg_{water}$, denoted herein as g/kg. In each experiment new 1.5 mL glass vials (VWR 548-0018) were used. Vials were washed with deionized water and dried prior to the preparation of the solutions. The required amount of glycine powder was weighed directly into the glass vials, and 1 mL of deionized water was pipetted into each vial. For the oil-interface experiments, 200 μL of tridecane was then pipetted on top of the water to create an oil−solution interface.

The vials were then transferred to a Polar Bear Plus Crystal. The Polar Bear is a precision heating and cooling platform produced by Cambridge Reactor Design that uses interchangeable plate attachments to allow for accurate (±0.1 °C) temperature control for a range of vessels from vials to round-bottom flasks. The vials were held overnight to fully dissolve the glycine. The solutions prepared at 275−365 g/kg were held at 343 K, while those prepared at 400−450 g/kg were held at 363 K to ensure that they were safely below the solubility of γ-glycine, which is poorly reported in the literature with few sources with contradictory results.[23] A total of 40 vials were prepared at each concentration of 275, 307, 333, 365, 400, and 450 g/kg without the oil interface, and 80 vials were prepared at each concentration of 275, 307, 333, and 365 g/kg with the oil interface.

The vials were checked visually to ensure that the glycine had fully dissolved and were then cooled in the Polar Bear at a controlled rate of 1.5 K/min to 298 K. The vials were then transferred into vial racks placed within an incubator set to 298 K for temperature control. Webcams were used to capture images of the vials every 5 min to allow for the crystallization induction time of the vials to be measured. The experiments were observed at 298 K for 72 h.

In method two we prepared the samples using a stock solution. A 307 g/kg stock solution was prepared by weighing the required amounts of glycine and deionized water into a 100 mL glass bottle with a magnetic stirrer and sealed. A 200 μL aliquot of oil was pipetted into 40 prewashed and dried glass vials and were left in an incubator at 333 K along with the solution, which was stirred overnight using a magnetic stirrer. Solution was then pipetted from the bottle into each vial on top of the tridecane, with the solution sinking below the layer of oil. A fresh preheated pipette tip was used for each vial and pipetting was performed inside the incubator in order to prevent any crystallization occurring during the solution transfer process. Due to temperature limits of the incubator, solution preparation and transfer were carried out at 333 K. To ensure that any crystals that might have formed during the preparation method were redissolved, the vials were transferred to the Polar Bear at 343 K where they were held for 2 h before being cooled at a controlled rate of 1.5 K/min, transferred to the incubator at 298 K, and observed via webcam as described above.

In order to investigate the effects of the volumes of solution and oil, a number of experiments were performed using method two described above at varying oil−solution volume ratios. In all experiments the total volume of both the oil and solution combined was 1.2 mL (to match the previous experiments). Oil−solution volume ratios of 1:5, 1:1, and 2:1 were prepared at a glycine concentration of 307 g/kg. A total of 40 vials were prepared in each experiment.

Once a crystal formed within a vial, it was removed from solution and left at room temperature for 1 day to dry. The crystals were then ground to a powder, and the polymorph was determined using infrared (IR) spectroscopy. IR spectra were obtained using an ABB MB3000 spectrometer at a resolution of 1 cm^{-1}. Absorbance spectra were averaged over eight scans in the wavenumber range 700−1000 cm^{-1}. All spectra were collected at ambient temperatures. The poylmorphic form was identified using a key spectral region between 700 and 1000 cm^{-1}. The α polymorph can be identified by a characteristic peak at 910 cm^{-1}, while γ is identified by a peak at 927 cm^{-1}. Both polymorphs share a common peak at 887 cm^{-1}. Example spectra are provided in the Supporting Information.

MD simulations of glycine aqueous solutions at vacumm or tridecane interfaces were performed using the LAMMPS MD code.[24] For glycine, we used the Generalized AMBER Force Field (GAFF)[25] with CNDO charges, which was found to give the best results for crystalline α glycine, glycine solutions, and α glycine in contact with a supersaturated solution.[26] The

https://dx.doi.org/10.1021/acs.jpclett.0c00540
J. Phys. Chem. Lett. 2020, 11, 2263−2271

SPC/E water model[27] was used as recommended in the previous study as it was found to accurately represent the density and diffusion coefficients within the system. For tridecane we used the AMBER-ii force field that was developed for alkanes by Nikitin et al.[28] The force field parameters are given in the Supporting Information.

Three different systems were simulated: one with glycine solution−tridecane interfaces; one with glycine solution−vacuum interfaces, which represents the solution−air interface in the control experiments; a mixed-interface system with a solution−tridecane interface on one side and a solution−vacuum interface on the other. In all three cases, simulations were performed at 250 and 307 g/kg. The glycine solutions contained 240 glycine and 4000 water molecules for 250 g/kg and 295 glycine and 4000 water molecules for 307 g/kg. Visualizations of the systems, produced using the VMD software,[29] are shown in Figure 3.

The solution−tridecane system was prepared by placing two pre-equilibrated tridecane layers in contact with a box of glycine solution at either 250 or 307 g/kg. The tridecane layers were prepared by simulating 128 tridecane molecules in the *NVT* ensemble for 1 ns, followed by 1.2 ns in the *NPT* ensemble. The simulation box was then modified to the desired cross section (3.45 × 3.45 nm in the *xy* directions), energy minimized with an energy tolerance (relative change in energy) of 1.0×10^{-6} and a force tolerance of 1.0×10^{-6} kcal mol^{-1} $Å^{-1}$, and then simulated for a further 1 ns in *NPT*. A layer of tridecane was placed above and below the glycine solution box in the *z* direction, and a further energy minimization was performed. This combined system was then simulated for 0.2 ns in the *NVT* ensemble followed by 3.8 ns in *NPT* to equilibrate the system. A production run of 200 ns of *NPT* simulation was then performed.

The air−solution system used the same starting configurations of the glycine solution as the oil−solution system without the tridecane molecules added to either side. The total length of the box in the *z* direction was 30 nm. An energy minimization was performed followed by 4 ns of *NVT* dynamics for equilibration. This was followed by a 200 ns *NVT* production run.

The mixed-interface system was prepared by placing two pre-equilibrated tridecane layers, to increase the oil thickness, below the glycine solutions and a vacuum above the glycine solution and below the tridecane. An energy minimization was performed followed by 4 ns of *NVT* dynamics for equilibration. This was followed by a 200 ns *NVT* production run.

Simulations of the oil−solution interface were performed in the *NPT* ensemble while maintaining the *x* and *y* dimensions at 3.45 nm and allowing the box to vary only in the *z* direction to maintain the pressure. The air−solution-interface simulation was performed in the *NVT* ensemble with the same *x* and *y* dimensions of the oil−solution simulation. For *NPT* simulations the temperature and pressure were maintained at 298 K and 1 atm using a Nose−Hoover thermostat and barostat with damping parameters of 1 and 2 ps for temperature and pressure, respectively. For the *NVT* simulations the temperature was maintained at 298 K using a Nose−Hoover thermostat with a damping parameter of 1 ps. Lennard-Jones interactions were truncated at a cutoff of 1.4 nm, while short-range electrostatics were calculated below 0.98 nm. Long-range electrostatics were calculated using a particle−particle−particle−mesh with an accuracy of 1×10^{-6}. Lennard-Jones 1−4 interactions were reduced to 0.5, while electrostatic 1−4 interactions were reduced to 0.833 as intended for AMBER style force fields. All simulations were performed using a time step of 2.0 fs. Thermodynamic properties were sampled every 200 fs, while structural information was sampled every 20 ps.

Structural property profiles perpendicular to the oil−solution and air−solution interfaces have been calculated. The simulation box was separated into bins, and for each snapshot the position of each atom or molecule, as appropriate, was placed into the bin associated with its fractional position of the box for that time step. To account for drifting of the interfaces in the *z* direction, the *z* component of the center-of-mass (COM) of the solution phase was calculated at each time step and distances were calculated from this point.

First, we show experimentally that the presence of the oil−solution interface has a dramatic effect on the nucleation kinetics of glycine from aqueous solution. We then present computational results that show that local compositions of glycine aqueous solutions in the vicinity of air−solution and oil−solution interfaces are significantly different from those in the bulk solution. We then outline a general argument for how interfaces influence heterogeneous nucleation from solutions through inducing local concentration heterogeneity near the interface, which is a novel effect distinct from and complementary to heterogeneous nucleation mechanisms previously proposed in literature.

Nucleation kinetics were assessed by monitoring induction times in vials holding glycine solutions prepared under controlled cooling conditions and then held isothermally for up to 72 h. Glycine solutions in vials with the layer of tridecane on the top were found to be readily nucleating at moderate glycine concentrations, 275, 307, 333, and 365 g/kg (corresponding to relative supersaturations of 1.36, 1.52, 1.65, and 1.81 with respect to the solubility of γ-glycine[30]) where 60, 89, 94, and 93% of the vials nucleated, respectively, within 72 h at 298 K (see Figure 1). It was observed that crystals were typically forming at the oil−solution interface. However, vials without the oil layer were found to have much lower probability of nucleation under the same conditions.

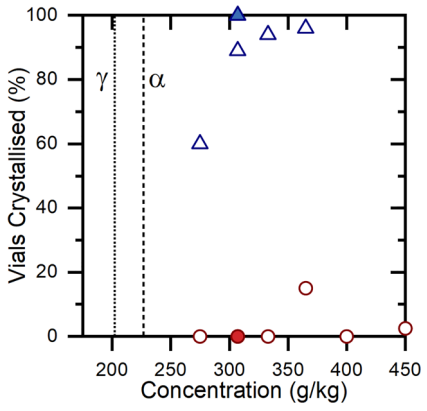

Figure 1. Percentage of vials where glycine crystallized within 72 h. Red symbols represent experiments with an air−solution interface and blue symbols represent experiments with an oil−solution interface. Open symbols represent experiments run using sample preparation method one while filled symbols represent sample preparation method two. Note that experiments with the oil interface were only performed for concentrations below 400 g/kg. The lines represent γ and α solubilities of 202 and 227 g/kg at 298 K, respectively.[30]

https://dx.doi.org/10.1021/acs.jpclett.0c00540
J. Phys. Chem. Lett. 2020, 11, 2263−2271

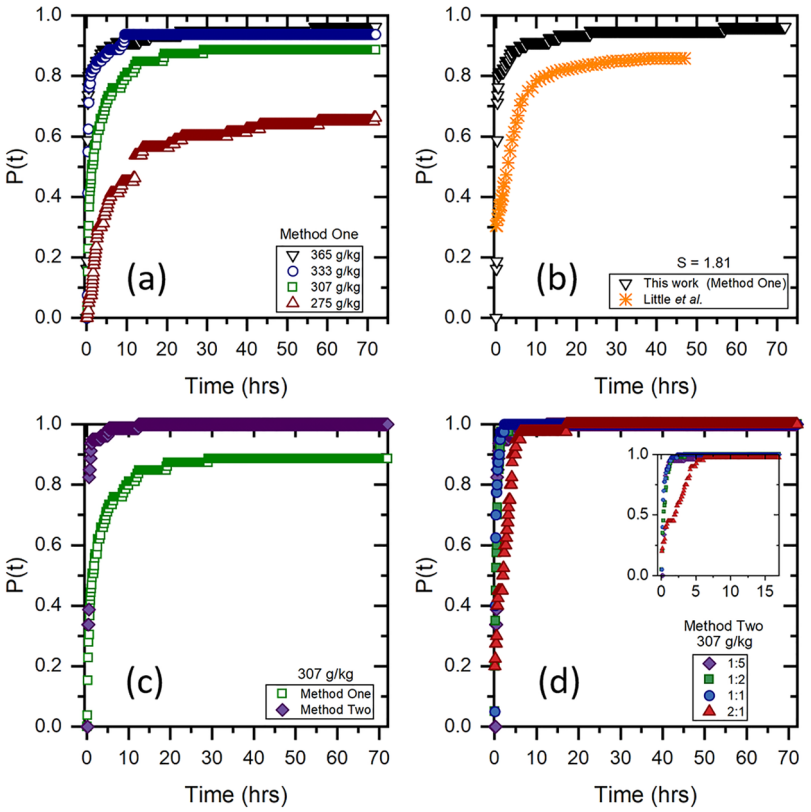

Figure 2. Cumulative probability distribution function of induction times of glycine crystallization from aqueous solution with a tridecane interface for (a) different concentrations prepared using method one, (b) relative supersaturation of 1.81 with respect to γ-glycine (365 g/kg at 298 K prepared using method one and 333 g/kg at 294 K from work of Little et al.[20]), (c) 307 g/kg prepared using methods one and two, and (d) 307 g/kg prepared using method two with different oil–solution volume ratios.

This is in agreement with our previous work, where the probability of nucleation in glycine solutions was very low at concentrations below 475 g/kg using the same condition and preparation procedures (sample preparation method two).[23] Similar results were obtained when using a different solution preparation procedure (sample preparation method two), as can be seen in Figure 1. These results clearly demonstrate that the oil–solution interface has a dramatic influence on the kinetics of glycine nucleation.

From the oil–solution-interface systems that nucleated we see a similar polymorphic distribution regardless of the concentration. The overall polymorphic distribution obtained from the 218 samples analyzed from the oil–solution-interface experiments was 94% α, 1% γ, and a 5% mixture of the two polymorphs. Of the seven samples that nucleated from the air–solution-interface systems five were α, one was γ, and one was a mixture of the two polymorphs. It appears that the oil does not significantly change the polymorph selection; however, we note that there are insufficient air–solution-interface samples for statistical significance.

Cumulative distribution functions $P(t)$ of induction times obtained using sample preparation method one are shown in Figure 2a. In all cases we see similar behavior, with a significant fraction of vials nucleating within first few hours, followed by a smaller fraction of vials nucleating within next few days, leaving a number of vials without any visible crystals after 3 days. The nucleation probability increases with concentration, as expected. However, it can be clearly seen that the nucleation probability $P(t)$ does not follow a Poisson distribution time dependence $P(t) = 1 - \exp(-JV(t - t_g))$ where J is the nucleation rate, V is the volume of solution, and t_g is the growth time, which would correspond to the expected stochastic outcome for a constant nucleation rate.[31] This nucleation probability behavior is consistent with those seen in previous studies of glycine nucleation under quiescent (nonagitated) conditions.[20,23,32] We note that sample preparation method two does not lead to this phenomenon (see Figure 2c). One possible reason is that the contact time between oil and solution is greater in method one than in method two, which suggests that there may be a time-dependent effect that acts to hinder nucleation occurring at longer times, for example an impurity present that, given enough time, poisons the interface, thus resulting in non-Poisson behavior.

In Figure 2b we show combined results from three experimental runs performed by Little et al.[20] which were obtained with a different setup, but using a layer of tridecane at the top of glycine with the same relative supersaturation (Little: 333 g/kg at 294 K, present work: 365g/kg at 298 K, with relative supersaturations of 1.81 relative to γ-glycine). Our experiments had somewhat higher probabilities of nucleation than those observed by Little et al.: we saw 81% of the samples nucleating within the first hour and 95% nucleating within 2 days, as compared to 52% and 79% nucleating at within the same time frames respectively, observed by Little et al. Although using the same supersaturation, there were a number of differences between the experiments performed in both cases, in addition to slightly different temperature. Our samples had a greater volume of solution (1 mL vs 100 μL), greater volume of oil (200 μL vs 100 μL), and greater interfacial

https://dx.doi.org/10.1021/acs.jpclett.0c00540
J. Phys. Chem. Lett. 2020, 11, 2263–2271

surface area (64 mm^2 vs 38 mm^2). Our samples were held in glass vials, while Little held their samples in treated polystyrene microplate wells. The increased volume of solution in our samples would result in reduced induction times for (bulk based) nucleation, while the increased interfacial surface area would reduce the induction time for heterogeneous nucleation at the interface. The increased volume of oil would only be expected to impact the induction time if impurities present within the oil influence nucleation.

Little et al. also suggested that nucleation observed within 60 min of solution addition to microplate wells containing supersaturated glycine solution may have been due to disturbances introduced by the addition of solution. However, in our case solutions were prepared with oil added before heating so that any crystals formed should be dissolved before the vials were cooled and so artifacts like those proposed by Little et al. would have been avoided. Nevertheless, many vials nucleated within the first 60 min in our experiments, similar to those in experiments of Little et al.

In Figure 2c we show the effect of the sample preparation method (methods one vs method two) used in our work. The samples prepared individually within the glass vials (method one) had lower nucleation probabilities than those prepared using a stock solution (method two) and all vials nucleated within a day when using the stock solution method. This highlights the importance of accounting for preparation method and thermal history of samples in nucleation studies in order to get accurate quantitative nucleation kinetic data.[33] However, regardless of preparation method, glycine nucleation is clearly strongly accelerated in the presence of the oil−solution interface.

To further confirm that the oil−solution interface is the cause of accelerated nucleation, we investigated a range of oil to solution volume ratios while keeping the surface area of the oil−solution-interface constant. In these experiments the samples have the same total volume of solution and oil combined, and the same oil−solution interfacial area, but with varying oil to solution ratios. The induction times obtained for each ratio are shown in Figure 2d. We can see that distributions of induction times are very similar for oil to solution volume ratios 1:5 (the original one), 1:2 and 1:1. The total volume for the samples with different oil to solution volume ratio was held constant, and, therefore, the volume of the glycine solution, and the glass-solution interfacial area were different for each ratio. If the overall nucleation rate was proportional to the solution volume, we would expect that the nucleation rate would scale with the solution volume in a given vial, and thus with oil−solution ratio in our experiments. However, in Figure 2d, it is clear that the overall nucleation rate does not change significantly. This is what would be expected if nucleation is controlled by the oil−solution interfacial area, which is constant, rather than the solution volume (or glass−solution interfacial area).[34] We note that somewhat longer induction times were recorded at the ratio of oil to solution volume ratio 2:1, which may be due to an onset of concentration depletion as the solution volume become smaller, slowing down crystal growth so that crystal detection takes somewhat longer, while it can still be seen that all vials nucleated in less than 10 h. Our observations also rule out that nucleation would be due to impurities in oil as increasing volume of oil does not lead to faster nucleation.

In our recent work, we reported that PTFE coated magnetic stirrer bar placed in glycine aqueous solution without agitation was also found to strongly promote glycine nucleation.[23] We note that both PTFE and tridecane used in this work are hydrophobic and both of these interfaces enhance glycine nucleation. Di Profio et al.[35] investigated effects of polymer surfaces on heterogeneous nucleation from solution and concluded that chemical functionalities of the polymer surface dictate whether the surface promotes enhanced nucleation. Under similar conditions to our lower concentrations (Di Profio, 180.2 g/kg at 278 K; present work, 275 g/kg at 298 K, with relative supersaturations of 1.42 and 1.36, respectively, relative to γ-glycine), they found that hydrophilic polymers enhanced glycine nucleation from aqueous solutions in contrast to hydrophobic polymers (PP, co-PVDF). However, it is likely that wetting issues due to significant surface roughness may have been paramount in their work as reported by Di Profio.

To gain insight into the surface effects that contribute to enhancement of heterogeneous nucleation, we perform MD simulations of the oil−solution and air−solution interfaces to investigate the molecular level solution structure and dynamics near the interface.

Glycine aqueous solutions in contact with tridecane and/or air interfaces were investigated computationally using molecular dynamics simulations in order to determine local composition as well as the orientation of glycine near these interfaces. We simulated the glycine solutions at two different concentrations of 250 g/kg and 307 g/kg. Both concentrations correspond to supersaturated solutions with respect to the solubility of α-glycine (227 g/kg at 298 K[30]), which is relevant as most of our samples crystallized in the α form. The simulation box resulted in an average z length of 20.2 nm for the glycine solution film.

The density profile of each component within the simulated interface systems in the z direction perpendicular to the interface are shown in Figure 3. It can be seen that there is a strong enhancement in the glycine density occurring in an interfacial region near the oil−solution interface, while at the air−solution interface there is a strong depletion in the glycine density. We indicate interfacial regions with thickness of 1 nm to highlight that glycine density enhancement extends over length scales comparable to expected magnitude of crystal nuclei dimensions. Interfacial regions for the oil−solution system were defined from the point of highest glycine concentration (the ratio of the densities of glycine and water) at the interface and reach 1 nm toward the center of the glycine solution (see Supporting Information for more details). The interfacial regions for the air−solution interface were defined as having the same position as the oil−solution-interface system of the same concentration.

The average glycine concentrations in the interfacial regions are given in Table 1. The interfacial concentrations at the oil−solution interface are 1.21 and 1.26 times the overall system concentrations of 250 and 307 g/kg, respectively. However, the interfacial concentrations of the air−solution interface are 0.54 and 0.51 times the overall system concentrations.

The calculated glycine interfacial concentration of 386 g/kg at the oil−solution interface (corresponding to an overall concentration of 307 g/kg) is smaller than the glycine concentrations used in spontaneous nucleation experiments in the absence of oil.[23] At overall concentrations of 400 g/kg or below, glycine nucleation was extremely slow in the absence of oil. However, we note that nucleation was likely to be heterogeneous at the glass vial surface.[36] The interfacial

https://dx.doi.org/10.1021/acs.jpclett.0c00540
J. Phys. Chem. Lett. 2020, 11, 2263−2271

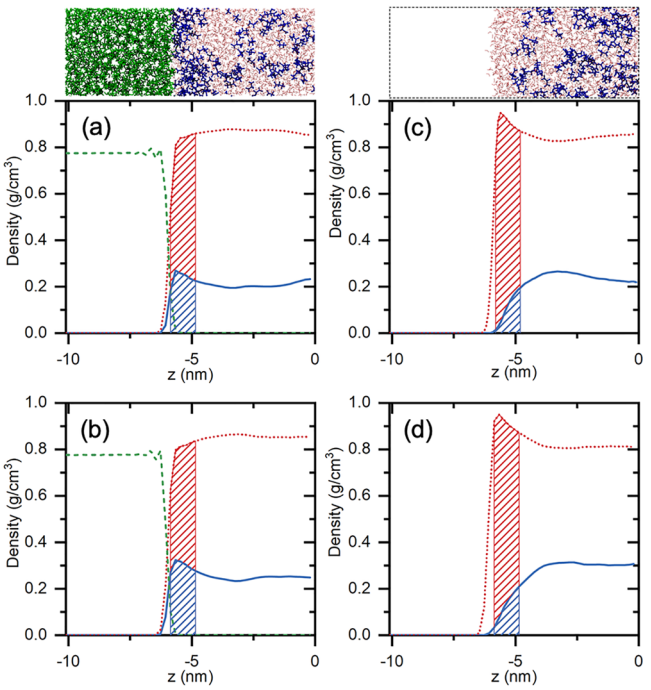

Figure 3. Density profiles of glycine (solid blue line), water (dotted red line), and tridecane (dashed green line) of the simulated oil–solution interfaces at (a) 250 g/kg and (b) 307 g/kg and air–solution interfaces at (c) 250 g/kg and (d) 307 g/kg in the z direction (perpendicular to the interface). The patterned areas show the 1 nm thick interface regions. The center-of-mass of the glycine solution is set to $z = 0$ and the data have been symmetrized over both interfaces. Snapshots of the interfaces are shown above with glycine (blue), water (red), and tridecane (green) molecules.

Table 1. Total and Interfacial Concentrations of Glycine at the Oil and Air Interfaces, with the Concentration Ratio Showing Enhancement and Depletion at the Oil and Air Interfaces, Respectively

system	total conc (g/kg)	interface conc (g/kg)	conc ratio
oil	250	303	1.26
air	250	136	0.54
oil	307	386	1.21
air	307	156	0.51

concentration at the glass surface is unknown and, as we have seen from our results for the oil and air interfaces, it cannot be directly inferred from the bulk concentration.

In order to ensure robustness of the calculated interfacial concentration effect, we performed three additional tests: we varied film thickness, used asymmetric films boundaries, and tested for concentration fluctuations.

First, we investigated how the finite size of the film affects the concentration profile, as the finite size may act to reduce the enhanced interfacial concentration at the oil interface, due to depletion of glycine in the center of the thin film. Conversely, the concentration at the air interface may be higher due to the finite size of the film. We performed a 200 ns run of a thinner film of approximately 6 nm between two oil interfaces for a concentration of 307 g/kg. As expected, the interfacial concentration enhancement was smaller with an interfacial concentration of 344 g/kg corresponding to a concentration ratio of 1.12. In vial-based experiments there would be an effectively infinite reservoir of glycine solution when compared to the size of the interfacial region, and, therefore, it can be expected that the interfacial concentration effects would be even more significant under typical experimental conditions.

As air and oil interfaces have opposite effects on the interfacial glycine concentration, a third system was constructed containing an oil–solution interface on one side and an air–solution interface on the other. It was expected that the increase in glycine concentration in the central region due to the air–solution interface would at least partially cancel the depletion of glycine in the central region due to the oil–solution interface. The density profiles obtained are shown in Figure 4. The same effects can be observed at each of the

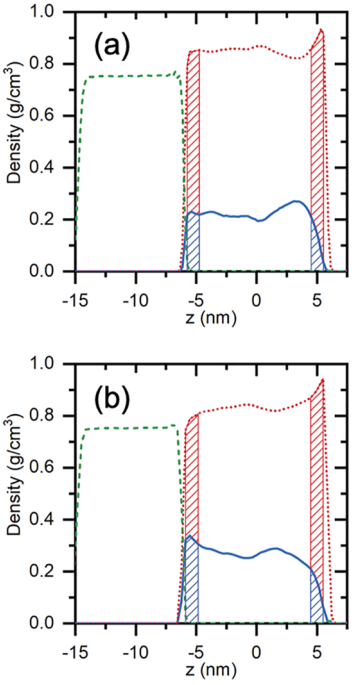

Figure 4. Density profiles of glycine (solid blue line), water (dotted red line), and tridecane (dashed green line) of the double-interface system at (a) 250 g/kg and (b) 307 g/kg in the z direction. The patterned areas show the 1 nm thick interface regions. There is a vacuum layer on the right of the glycine solution (not shown).

interfaces as seen previously. The double-interface simulation results in an interfacial concentration of 1.33 times the overall concentration at the oil interface, and an interfacial concentration of 0.54 times the overall concentration for the air interface, for the overall concentration of 307 g/kg. We obtain similar results for a glycine concentration of 250 g/kg, with a concentration ratio of 1.06 and 0.44 at the oil and air interfaces, respectively.

We note that there are concentration fluctuations in the center of the glycine solution film, as seen in Figure 3. These fluctuations are still present after relatively long simulation times (200 ns of production) and efforts were undertaken to improve sampling. For a solution concentration of 250 g/kg we used the same minimized, pre-equilibration starting configuration, applied an independent set of velocities to the atoms, and used the same equilibration procedure as described previously, followed by a 10 ns production run. This process was repeated 10 times to provide a combined total of 100 ns simulation time from independent starting configurations.

https://dx.doi.org/10.1021/acs.jpclett.0c00540
J. Phys. Chem. Lett. 2020, 11, 2263–2271

Interfacial concentration deviations are consistently present in all cases, giving an average interfacial concentration of 265 g/kg, corresponding to a concentration ratio of 1.06. This demonstrates that the enhanced concentration at the oil−solution interface is not due to fluctuations, which can be observed in the center of the film. The density profiles obtained for each short run along with the average of all 10 runs are shown in the Supporting Information.

The contrasting effects of the oil and air interfaces on the interfacial concentration highlight that heterogeneous nucleation rates can be expected to vary significantly among different interfaces, even in the absence of specific interactions. We note that this is in the absence of templating, physical confinement, or specific chemical interactions, which have been customarily implicated in heterogeneous nucleation mechanisms. Depletion of glycine near the air−solution interface is also consistent with surface tension measurements of aqueous glycine solutions.[37] The increase in glycine concentration at the oil−solution interface is not a surfactant effect, as glycine is zwitterionic and not amphiphilic. However, it is known that large, polarizable ions have an affinity for a water−oil interface due to cavitation and dispersion forces, whereas smaller ions remain hydrated.[38] By analogy with this effect, we believe that the enhanced interfacial concentration is likely due to nonspecific van der Waals interactions between the interface material and the solute or solvent molecules. Specifically, for glycine aqueous solution, the van der Waals interaction between glycine and tridecane is significantly stronger than the van der Waals interaction between water and tridecane, leading to enhanced glycine interfacial concentration at the tridecane−solution interface. The same argument can also explain the enhanced nucleation of glycine that was previously seen at the liquid−solid interface of a PTFE stirrer bar.[23]

Molecular orientation at the interface is one of the underlying mechanisms that can lead to an increased heterogeneous nucleation rate. To investigate this effect, we have examined the orientation of the glycine molecules at the interface using the bond orientation parameter P_2:

$$P_2 = \frac{3}{2}\langle \cos^2\theta \rangle - \frac{1}{2} \quad (1)$$

where θ is the angle between the z-axis and the C−C bond vector. A P_2 value of 1.0 corresponds to the C−C bond being oriented perpendicular to the interface, while a value of −0.5 indicates the bond lies parallel to the interface. A P_2 value of 0 corresponds to random bond orientations. We have investigated the variation of the bond order with distance from the interface, taking the position of the molecule as its COM. The bond orientation profiles for the air and oil interfaces can be seen in Figure 5. For both the air and oil interfaces, it can be seen that the glycine molecule C−C bonds are mainly oriented parallel to the interface, with the orientation becoming random toward the center of the solution. We also note that the orientation profiles at the air and oil interfaces are very similar, indicating that the orientation is mainly a steric or packing effect, rather than due to a specific interaction. While P_2 generally decreases within the interfacial region, there is a point in each graph where the value increases to above 0. These points occur where the glycine density is less than 2×10^{-3} g cm^{-3}, and so they are not statistically relevant.

The local translational and rotational mobility of the glycine molecules was also investigated in order to determine if there was physisorption of the glycine at the interface. The mean

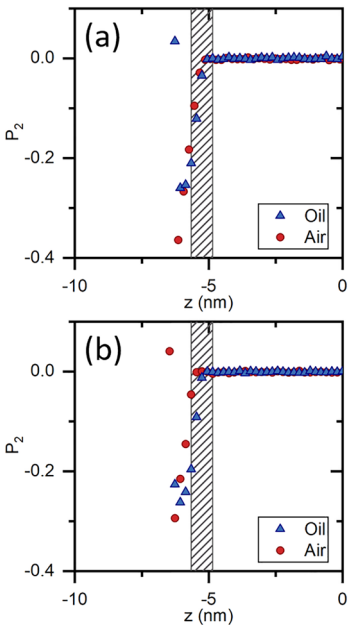

Figure 5. Bond orientation profile in the z direction of the C−C bond vector of glycine at (a) 250 g/kg and (b) 307 g/kg for an air interface (red circles) and oil interface (blue triangles). The patterned areas show the 1 nm thick interface regions.

squared displacement (MSD) in the x and y directions (parallel to the interface) of the molecules in the interfacial region was compared to that of the molecules in the center of the solution. As we are interested in a 1 nm region, the MSD in the z direction is not a useful metric for examining the mobility of the molecules perpendicular to the interface and, instead, we compared the length of time a molecule remains within the interfacial region to the length of time they spend within a region of the same size in the center of the film. To determine the rotational mobility of the molecules, the autocorrelation function (ACF) of the C−C bond vector of the glycine molecules was calculated for molecules while they were within the interfacial region and compared to that of the molecules in the center of the solution. At each of the oil interfaces, we find there is a slight reduction in the mobility of the glycine molecules within the interfacial regions, although this would be expected in a region of higher concentration.[26] However, the molecules remain highly mobile and are not adsorbed at the interface. This is in contrast to previously observed effects such as Barite epitaxial growth that showed the water monolayer formation on a Barite surface,[39] where the adsorbed water creates a barrier for barium and sulfate ions approaching the surface. The MSD, ACF, and lifetime analysis for glycine in the interfacial and central regions of the solution film can be found in the Supporting Information.

In this work we investigated the impact of an oil−solution interface on the nucleation kinetics of glycine. Experimentally, we observed that there is a vast increase in the nucleation rate in the presence of an oil−solution interface, compared to vials with an air−solution interface. This is surprising as the hydrophobic oil would not be expected to enhance the heterogeneous nucleation of polar glycine. Current mechanisms widely used in the literature to describe the enhanced rate at which heterogeneous nucleation occurs, such as physical and chemical templating, do not apply to this system due to

https://dx.doi.org/10.1021/acs.jpclett.0c00540
J. Phys. Chem. Lett. 2020, 11, 2263−2271

the absence of specific functional groups and the liquid nature of the interface.

MD simulations were used to gain insight into the solution structure at the interface and they revealed an enhanced concentration and ordering of the glycine molecules at the oil−solution interface. Similar simulations of the air−solution interface demonstrate the opposite effect with a greatly reduced glycine concentration. These effects are likely due to nonspecific net van der Waals interactions between the tridecane−water and tridecane−glycine, which compete with solution interactions to determine the interfacial concentration profiles.

While these effects were observed for glycine solutions at a tridecane interface, we expect that the same mechanism will be present in a wide range of solution-interface systems. This new insight will allow us to control interfacial concentration in order to design effective nucleants for the enhancement of nucleation, but also to prevent heterogeneous nucleation in antifouling applications.

■ ASSOCIATED CONTENT

Supporting Information

The Supporting Information is available free of charge at https://pubs.acs.org/doi/10.1021/acs.jpclett.0c00540.

> Discussion of nucleation experiments and polymorphic identification (including tables of solubilities, experimental conditions and a graph of IR spectra); discussion of simulation details, including force field parameters, definition of interfacial regions, sampling, and interfacial dynamics (including tables of force field parameters, GAFF atom structure, and graphs of autocorrelation functions, mean square displacements, and density profiles) (PDF)

■ AUTHOR INFORMATION

Corresponding Author

Karen Johnston − *Department of Chemical and Process Engineering, University of Strathclyde, Glasgow G1 1XJ, U.K.*; orcid.org/0000-0002-5817-3479; Email: karen.johnston@strath.ac.uk

Authors

David McKechnie − *Department of Chemical and Process Engineering and Doctoral Training Centre in Continuous Manufacturing and Advanced Crystallisation, University of Strathclyde, Glasgow G1 1XJ, U.K.*

Samira Anker − *Department of Chemical and Process Engineering, University of Strathclyde, Glasgow G1 1XJ, U.K.*

Saraf Zahid − *Department of Chemical and Process Engineering, University of Strathclyde, Glasgow G1 1XJ, U.K.*

Paul A. Mulheran − *Department of Chemical and Process Engineering, University of Strathclyde, Glasgow G1 1XJ, U.K.*

Jan Sefcik − *Department of Chemical and Process Engineering and EPSRC Future Manufacturing Research Hub in Continuous Manufacturing and Advanced Crystallisation, University of Strathclyde, Glasgow G1 1XJ, U.K.*

Complete contact information is available at: https://pubs.acs.org/10.1021/acs.jpclett.0c00540

Notes

The authors declare no competing financial interest.

Raw experimental data and simulation input files are available at doi.org/10.15129/846b26c2-7040-4c71-b1a8-aa2f9cbe1bba.

■ ACKNOWLEDGMENTS

The authors thank EPSRC and the Future Manufacturing Research Hub in Continuous Manufacturing and Advanced Crystallization (Grant ref: EP/P006965/1) for funding this work. We also acknowledge that this work was carried out in the CMAC National Facility supported by UKRPIF (UK Research Partnership Investment Fund) award from the Higher Education Funding Council for England (HEFCE) (Grant ref: HH13054). Additional funding for the computational work was provided by The Carnegie Trust for the Universities of Scotland (Grant ref: R1G007756). Results were obtained using the EPSRC funded ARCHIE-WeSt High Performance Computer (www.archie-west.ac.uk) EPSRC grant number EP/K000586/1.

■ REFERENCES

(1) Campbell, James M.; Meldrum, Fiona C.; Christenson, Hugo K. Observing the formation of ice and organic crystals in active sites. *Proc. Natl. Acad. Sci. U. S. A.* **2017**, *114* (5), 810−815.

(2) Gettelman, A.; Liu, X.; Ghan, S. J.; Morrison, H.; Park, S.; Conley, A. J.; Klein, S. A.; Boyle, J.; Mitchell, D. L.; Li, J.-L. F. Global simulations of ice nucleation and ice supersaturation with an improved cloud scheme in the community atmosphere model. *J. Geophys. Res.* **2010**, *115*, D18216.

(3) Van Driessche, A. E. S.; Van Gerven, N.; Bomans, P. H. H.; Joosten, R. R. M.; Friedrich, H.; Gil-Carton, D.; Sommerdijk, N. A. J. M.; Sleutel, M. Molecular nucleation mechanisms and control strategies for crystal polymorph selection. *Nature* **2018**, *556* (7699), 89−94.

(4) Khan, Saeed R.; Pearle, Margaret S.; Robertson, William G.; Gambaro, Giovanni; Canales, Benjamin K.; Doizi, Steeve; Traxer, Olivier; Tiselius, Hans-Goran Kidney stones. *Nat. Rev. Dis. Primers* **2016**, *2* (1), 16008.

(5) Pande, Ajay; Pande, Jayanti; Asherie, Neer; Lomakin, Aleksey; Ogun, Olutayo; King, Jonathan; Benedek, George B. Crystal cataracts: Human genetic cataract caused by protein crystallization. *Proc. Natl. Acad. Sci. U. S. A.* **2001**, *98* (11), 6116−6120.

(6) Blagden, N.; de Matas, M.; Gavan, P. T.; York, P. Crystal engineering of active pharmaceutical ingredients to improve solubility and dissolution rates. *Adv. Drug Delivery Rev.* **2007**, *59* (7), 617−630.

(7) Davey, R. J.; Schroeder, S. L. M.; ter Horst, J. H. Nucleation of Organic Crystals—A Molecular Perspective. *Angew. Chem., Int. Ed.* **2013**, *52* (8), 2166−2179.

(8) Parambil, Jose V.; Poornachary, Sendhil K.; Heng, Jerry Y. Y.; Tan, Reginald B. H. Template-induced nucleation for controlling crystal polymorphism: from molecular mechanisms to applications in pharmaceuticals processing. *CrystEngComm* **2019**, *21* (28), 4122−4135.

(9) Diao, Y.; Myerson, A. S.; Hatton, T. A.; Trout, B. L. Surface design for controlled crystallization: The role of surface chemistry and nanoscale pores in heterogeneous nucleation. *Langmuir* **2011**, *27* (9), 5324−5334.

(10) Mitchell, C. A.; Yu, L.; Ward, M. D. Selective nucleation and discovery of organic polymorphs through epitaxy with single crystal substrates. *J. Am. Chem. Soc.* **2001**, *123* (44), 10830−10839.

(11) Diao, Y.; Whaley, K. E.; Helgeson, M. E.; Woldeyes, M. A.; Doyle, P. S.; Myerson, A. S.; Hatton, T. A.; Trout, B. L. Gel-induced selective crystallization of polymorphs. *J. Am. Chem. Soc.* **2012**, *134* (1), 673−684.

(12) Laval, Philippe; Salmon, Jean-Baptiste; Joanicot, Mathieu A microfluidic device for investigating crystal nucleation kinetics. *J. Cryst. Growth* **2007**, *303* (2), 622−628.

(13) Shim, J.-u.; Cristobal, G.; Link, D. R.; Thorsen, T.; Fraden, S. Using microfluidics to decouple nucleation and growth of protein crystals. *Cryst. Growth Des.* **2007**, *7* (11), 2192−2194.
(14) Teychené, Sébastien; Biscans, Béatrice Microfluidic device for the crystallization of organic molecules in organic solvents. *Cryst. Growth Des.* **2011**, *11* (11), 4810−4818.
(15) Ildefonso, Manuel; Candoni, Nadine; Veesler, Stéphane A cheap, easy microfluidic crystallization device ensuring universal solvent compatibility. *Org. Process Res. Dev.* **2012**, *16* (4), 556−560.
(16) Riechers, Birte; Wittbracht, Frank; Hütten, Andreas; Koop, Thomas The homogeneous ice nucleation rate of water droplets produced in a microfluidic device and the role of temperature uncertainty. *Phys. Chem. Chem. Phys.* **2013**, *15* (16), 5873−5887.
(17) Akella, Sathish V.; Mowitz, Aaron; Heymann, Michael; Fraden, Seth Emulsion-based technique to measure protein crystal nucleation rates of lysozyme. *Cryst. Growth Des.* **2014**, *14* (9), 4487−4509.
(18) Dombrowski, Richard D.; Litster, James D.; Wagner, Norman J.; He, Yinghe Crystallization of alpha-lactose monohydrate in a drop-based microfluidic crystallizer. *Chem. Eng. Sci.* **2007**, *62* (17), 4802−4810.
(19) Chayen, Naomi E.; Shaw Stewart, Patrick D.; Blow, David M. Microbatch crystallization under oil — a new technique allowing many small-volume crystallization trials. *J. Cryst. Growth* **1992**, *122* (1), 176−180.
(20) Little, Laurie J.; Sear, Richard P.; Keddie, Joseph L. Does the γ polymorph of glycine nucleate faster? A quantitative study of nucleation from aqueous solution. *Cryst. Growth Des.* **2015**, *15* (11), 5345−5354.
(21) Ildefonso, Manuel; Candoni, Nadine; Veesler, Stéphane Heterogeneous nucleation in droplet-based nucleation measurements. *Cryst. Growth Des.* **2013**, *13* (5), 2107−2110.
(22) Briuglia, M. L. Primary and Secondary Crystal Nucleation of Pharmaceutics. *Ph.D. thesis*, University of Strathclyde, Glasgow, 2017.
(23) Vesga, M. J.; McKechnie, D.; Mulheran, P. A.; Johnston, K.; Sefcik, J. Conundrum of γ glycine nucleation revisited: to stir or not to stir? *CrystEngComm* **2019**, *21*, 2234−2243.
(24) Plimpton, Steve Fast parallel algorithms for short-range molecular dynamics. *J. Comput. Phys.* **1995**, *117* (1), 1−19.
(25) Wang, Junmei; Wolf, Romain M.; Caldwell, James W.; Kollman, Peter A.; Case, David A. Development and testing of a general amber force field. *J. Comput. Chem.* **2004**, *25* (9), 1157−1174.
(26) Cheong, D. W.; Boon, Y. D. Comparative study of force fields for molecular dynamics simulations of α-glycine crystal growth from solution. *Cryst. Growth Des.* **2010**, *10* (12), 5146−5158.
(27) Berendsen, H. J. C.; Grigera, J. R.; Straatsma, T. P. The missing term in effective pair potentials. *J. Phys. Chem.* **1987**, *91* (24), 6269−6271.
(28) Nikitin, Alexei M.; Milchevskiy, Yury V.; Lyubartsev, Alexander P. A new AMBER-compatible force field parameter set for alkanes. *J. Mol. Model.* **2014**, *20* (3), 2143.
(29) Humphrey, William; Dalke, Andrew; Schulten, Klaus VMD − Visual Molecular Dynamics. *J. Mol. Graphics* **1996**, *14*, 33−38.
(30) Yang, Xia; Wang, Xiujuan; Ching, Chi Bun Solubility of form α and form γ of glycine in aqueous solutions. *J. Chem. Eng. Data* **2008**, *53* (5), 1133−1137.
(31) Jiang, S.; ter Horst, J. H. Crystal nucleation rates from probability distributions of induction times. *Cryst. Growth Des.* **2011**, *11* (1), 256−261.
(32) Javid, N.; Kendall, T.; Burns, I. S.; Sefcik, J. Filtration suppresses laser-induced nucleation of glycine in aqueous solutions. *Cryst. Growth Des.* **2016**, *16* (8), 4196−4202.
(33) Kuhs, Manuel; Zeglinski, Jacek; Rasmuson, Åke C Influence of history of solution in crystal nucleation of fenoxycarb: kinetics and mechanisms. *Cryst. Growth Des.* **2014**, *14* (3), 905−915.
(34) Sear, R. P. Quantitative studies of crystal nucleation at constant supersaturation: experimental data and models. *CrystEngComm* **2014**, *16*, 6506−6522.
(35) Di Profio, Gianluca; Fontananova, Enrica; Curcio, Efrem; Drioli, Enrico From Tailored Supports to Controlled Nucleation: Exploring Material Chemistry, Surface Nanostructure, and Wetting Regime Effects in Heterogeneous Nucleation of Organic Molecules. *Cryst. Growth Des.* **2012**, *12* (7), 3749−3757.
(36) Forsyth, C.; Burns, I. S.; Mulheran, P. A.; Sefcik, J. Scaling of glycine nucleation kinetics with shear rate and glass−liquid interfacial area. *Cryst. Growth Des.* **2016**, *16* (1), 136−144.
(37) Rodríguez, Diana M.; Romero, Carmen M. Surface Tension of Glycine, Alanine, Aminobutyric Acid, Norvaline, and Norleucine in Water and in Aqueous Solutions of Strong Electrolytes at Temperatures from (293.15 to 313.15) K. *J. Chem. Eng. Data* **2017**, *62* (11), 3687−3696.
(38) dos Santos, A. P.; Levin, Y. Ions at the Water−oil Interface Interfacial Tension of Electrolyte Solutions. *Langmuir* **2012**, *28* (2), 1304−1308.
(39) Piana, Stefano; Jones, Franca; Gale, Julian D. Assisted desolvation as a key kinetic step for crystal growth. *J. Am. Chem. Soc.* **2006**, *128* (41), 13568−13574.

https://dx.doi.org/10.1021/acs.jpclett.0c00540
J. Phys. Chem. Lett. 2020, 11, 2263−2271